Approximating the nonlinear density dependence of electron transport coefficients and scattering rates across the gas–liquid interface

APP Template V1.70 Article id: psstaaaa0c Typesetter: MPS Date received by MPS: 23/01/2018 PE: MAC004987 CE: LE:

IOP Publishing Plasma Sources Science and Technology

Plasma Sources Sci. Technol. **00** (2018) 000000 (14pp)

Approximating the nonlinear density dependence of electron transport coefficients and scattering rates across the gas–liquid interface

N A Garland[1], G J Boyle[1], D G Cocks[2] and R D White[1]

[1] College of Science & Engineering, James Cook University, Townsville, 4810, QLD, Australia
[2] Plasma Research Laboratories, Australian National University, Canberra, 2601, ACT, Australia

E-mail: nathan.garland@my.jcu.edu.au

Received 1 November 2017, revised 9 January 2018
Accepted for publication 23 January 2018
Published DD MM 2018

Abstract

This study reviews the neutral density dependence of electron transport in gases and liquids and develops a method to determine the nonlinear medium density dependence of electron transport coefficients and scattering rates required for modeling transport in the vicinity of gas–liquid interfaces. The method has its foundations in Blanc's law for gas-mixtures and adapts the theory of Garland *et al* (2017 *Plasma Sources Sci. Technol.* **26**) to extract electron transport data across the gas–liquid transition region using known data from the gas and liquid phases only. The method is systematically benchmarked against multi-term Boltzmann equation solutions for Percus–Yevick model liquids. Application to atomic liquids highlight the utility and accuracy of the derived method.

Keywords: interface, plasma–liquid, fluid model, structured media, momentum transfer theory, electron transport, common mean energy

1. Introduction

There has been a recent increase in the investigation of charged species transport across gas–liquid interfaces, with applications in environmental science, materials science, particle detector physics, plasma medicine, and electrical switching [1–3], of particular note is the change in the nature of particle transport due to changes in neutral background density[3]. The transition between a dilute gas and dense liquid involves many additional challenging phenomena such as surface tension, surface charge accumulation, and binding energy of electrons in a liquid [4, 5]. In this study, we choose to abstract the transport properties of intermediate fluid densities across the interface as a function of n_0, in order to facilitate modeling between the two distinct phases.

With a focus on plasma medicine advances, multiple studies have been performed in which charged particle transport in gases and liquids was governed by two separate sets of processes [1, 3, 5, 10, 11]. In these studies, gas and liquid models were coupled at a boundary [3, 11], or liquid interface effects were simply treated as a density and energy absorption or emission boundary condition applied to a gas phase model [1–3]. In addition, electromagnetic effects across the interface, such as permittivity changes and surface charge accumulation, have been included in previous comprehensive models [1, 3, 5, 10, 11].

In recent studies, it has been noted that further attention is required on the nature of electron transport in the gas–liquid interfacial region: (i) Lindsay *et al* [11] identified that a better understanding of interfacial electron transport may produce more accurate electron number density and energy loss emission/absorption coefficients for use in macroscopic transport models; (ii) while Mariotti *et al* [12] noted that radicals, ions, and photons are often considered when

[3] In this work we define the gas–liquid interface as an intermediate zone between homogeneous gas and liquid extremes, in which a well-defined increase in neutral density, n_0, from gas to liquid is observed [6–9].

studying plasma–liquid reactions, little attention has been given to electron interactions with the liquid phase. This current study seeks to develop a method for approximating electron transport properties across the gas and liquid phases to include the effects of nonlinear density dependent scattering processes from dilute gas to a dense liquid. A successful method will be capable of providing moment model [13] input data for electron transport at intermediate densities between two neutral particle density extremes, allowing future studies to more accurately model electron transport across a gas–liquid interface as a continuum over a neutral density transition.

In this study, we briefly review the formulation of moment models for electron transport in gases and liquids in section 2, elaborating on the modifications needed for electron transport in liquids. Section 2 also discusses the properties of a non-polar simple atomic liquid interface, and we explicitly highlight the input data requirements for modeling electron transport across an interface with a spatially varying neutral density. In section 3 we derive and benchmark approximate methods for a solution to the input data requirements, where benchmarking is performed for a simple model liquid. Application of the final proposed method is performed in section 4 using only electron drift velocities in the dilute gas and liquid phases. Assessment of the accuracy of the method is made for argon and xenon cases.

2. Theory

2.1. Moment modeling for electron transport in gases and liquids

Moment modeling is a common technique used to simulate a swarm or plasma, in gas or liquid media, via balance equations of velocity-averaged variables, such as density, momentum, and energy [13, 14–17]. This gives a relatively straightforward macroscopic model of a discharge, when compared to the complex mathematical and computational requirements of particle based methods such as partice-in-cell, Monte Carlo (MC), or kinetic solutions of the Boltzmann kinetic equation [16, 18–22]. The simplest variable in moment modeling is the number density of a species, defined as

$$n(\mathbf{r}, t) = \int f(\mathbf{r}, \mathbf{v}, t)\mathrm{d}\mathbf{v}, \tag{1}$$

where $f(\mathbf{r}, \mathbf{v}, t)$ is the electron velocity distribution function (EVDF).

Generic velocity moments can be then defined as

$$\langle\Phi\rangle(\mathbf{r}, t) = \frac{1}{n(\mathbf{r}, t)}\int f(\mathbf{r}, \mathbf{v}, t)\Phi(\mathbf{v})\mathrm{d}\mathbf{v}, \tag{2}$$

where $\Phi(\mathbf{v})$ is any velocity dependent function, and $\langle\ldots\rangle$ denotes the expectation value, a velocity average over $f(\mathbf{r}, \mathbf{v}, t)$.

Multiplying the Boltzmann equation by an arbitrary velocity dependent trial function $\Phi(\mathbf{v})$ and integrating over velocity space [16, 20] gives the generic moment equation

$$\frac{\partial}{\partial t}(n\langle\Phi\rangle) + \nabla\cdot(n\langle\mathbf{v}\Phi\rangle) - n\mathbf{a}\cdot\langle\nabla_{\mathbf{v}}\Phi\rangle = C_{\Phi}, \tag{3}$$

where $\mathbf{a}$ is the acceleration experienced by electrons due to applied electromagnetic fields, and C_{Φ} is the rate-of-change of $n\langle\Phi\rangle$ due to collisions.

Up to this point, the moment modeling methods described have been independent of the background media of the swarm or discharge. However, the collisional rate-of-change introduced in (3) is dependent on the medium and requires careful consideration of the coherent and incoherent scattering mechanisms within it [23, 24]

$$C_{\Phi} = C_{\Phi\,\mathrm{coherent}} + C_{\Phi\,\mathrm{incoherent}}. \tag{4}$$

In previous studies, the derivation [23, 24] and implementation [13] of structure dependent scattering into moment models has been presented through inclusions of elastic coherent scattering and electron interaction potential screening [25]. These effects are significant when the electron de Broglie wavelength is comparable to the average background particle spacing, $\lambda \sim n_0^{-\frac{1}{3}}$, and modifications to the electron collision frequencies used in moment modeling are derived.

It was shown that energy transfer collision rates, used in moment modeling, are not explicitly modified when coherent elastic scattering effects are included [23]. This allows the same form of equation to be used in dilute gas and soft condensed dense fluid background media [23, 24]. Energy transfer due to inelastic collisions is considered localized to the immediate target atom and is therefore unaffected by increased background densities, hence only the elastic scattering events require consideration in the formulation of a structure dependent kinetic theory. We note that other modifications to inelastic collisions can occur, such as collective excitations, however these remain incoherent and we do not consider them in this formulation.

In contrast to energy transfer, density dependent elastic coherent scattering produces explicit modifications to momentum transfer frequencies when the background medium is sufficiently dense, such as in a liquid [13, 23, 24]. The scattering effects due to increased densities of the background medium can be written as modifications of the dilute gas phase momentum transfer cross section

$$\sigma_m(v) = 2\pi\int_0^{\pi}\sigma(v, \chi)[1 - \cos\chi]\sin\chi\mathrm{d}\chi, \tag{5}$$

where v is the incoming electron speed, χ is the scattering angle from the target background medium, and $\sigma(v, \chi)$ is the gas phase differential cross section.

These structure modifications are implemented through a density dependent momentum transfer cross section

$$\Sigma_m(v, n_0) = 2\pi\int_0^{\pi}\Sigma(v, \chi, n_0)[1 - \cos\chi]\sin\chi\mathrm{d}\chi, \tag{6}$$

with $\Sigma(v, \chi, n_0)$ being an effective differential cross section including coherent scattering via

$$\Sigma(v, \chi, n_0) = \tilde{\sigma}(v, \chi)S(\Delta k, n_0), \tag{7}$$

where $\tilde{\sigma}(v, \chi)$ is the liquid phase differential cross section

containing any screening and polarization effects, $S(\Delta k, n_0)$ is the static structure factor and $\Delta k = \frac{2m_e v}{\hbar}\sin\frac{\chi}{2}$ is the wavenumber proportional to the change in momentum.

The static structure factor is a nonlinear function of n_0 of the target material, and may be calculated from molecular simulations, measured via experiments [23, 25, 26], or derived analytically through solutions of pair-correlation functions as per the Verlet–Weis structure factor [27]. For detailed discussion on the static structure factor, and its implementation in liquid scattering, readers are directed to previous studies [23, 25, 26].

Applying this framework for modifying the momentum transfer cross section, the momentum transfer frequencies for dilute gas and liquid scattering, used as input to moment models, are

$$\nu_m(v) = n_0 v \sigma_m(v), \tag{8}$$

$$\tilde{\nu}_m(v, n_0) = n_0 v \Sigma_m(v, n_0), \tag{9}$$

where $\nu_m(v)$ is the dilute gas momentum transfer frequency, and $\tilde{\nu}_m(v, n_0)$ is the structure modified momentum collision frequency. It should be noted that $\tilde{\nu}_m \to \nu_m$ in the limit of the electron de Broglie wavelength being much smaller than average background particle spacing, $\lambda \ll n_0^{-\frac{1}{3}}$.

Previously, moment models have been used to simulate electron transport in homogeneous media [13–15] in both gas and liquid phases. We now present the moment model used in this study, where space dependence of n_0 is explicitly included in the collision terms. Implementing the structure dependent scattering modifications, and the general moment integral (3), we can write a four moment model for electron transport, at any neutral density, where an electric field $\mathbf{E}$ is applied in the medium [13]

$$\frac{\partial n}{\partial t} + \nabla \cdot \mathbf{\Gamma} = n(\tilde{\nu}_I^{\mathrm{ss}}(\bar{\epsilon}, n_0) - \tilde{\nu}_a^{\mathrm{ss}}(\bar{\epsilon}, n_0)), \tag{10}$$

$$\frac{\partial \mathbf{\Gamma}}{\partial t} + \nabla \cdot (n\theta_m^{\mathrm{ss}}(\bar{\epsilon})) - n\frac{q_e}{m_e}\mathbf{E} = -\Gamma\tilde{\nu}_m^{\mathrm{ss}}(\bar{\epsilon}, n_0), \tag{11}$$

$$\frac{\partial n_\epsilon}{\partial t} + \nabla \cdot \mathbf{\Gamma}_\epsilon - q_e\mathbf{E} \cdot \mathbf{\Gamma} = -n\tilde{S}_\epsilon^{\mathrm{ss}}(\bar{\epsilon}, n_0), \tag{12}$$

$$\frac{\partial \mathbf{\Gamma}_\epsilon}{\partial t} + \nabla \cdot (n\theta_\xi^{\mathrm{ss}}(\bar{\epsilon})) - n\theta_m^{\mathrm{ss}}(\bar{\epsilon}) \cdot q_e\mathbf{E} - n_\epsilon\frac{q_e}{m_e}\mathbf{E} = -\Gamma_\epsilon\tilde{\nu}_\xi^{\mathrm{ss}}(\bar{\epsilon}, n_0), \tag{13}$$

where shorthand variables for particle flux Γ, energy density n_ϵ, and energy density flux Γ_ϵ are defined as

$$\Gamma = n\langle \mathbf{v} \rangle = \int f(\mathbf{r}, \mathbf{v}, t)\mathbf{v}\mathrm{d}\mathbf{v}, \tag{14}$$

$$n_\epsilon = n\bar{\epsilon} = \int f(\mathbf{r}, \mathbf{v}, t)\frac{1}{2}mv^2\mathrm{d}\mathbf{v}, \tag{15}$$

$$\Gamma_\epsilon = n\langle \boldsymbol{\xi} \rangle = \int f(\mathbf{r}, \mathbf{v}, t)\frac{1}{2}mv^2\mathbf{v}\mathrm{d}\mathbf{v}, \tag{16}$$

with $\langle \mathbf{v} \rangle$, $\bar{\epsilon} = \langle \epsilon \rangle$, and $\langle \boldsymbol{\xi} \rangle$ being the electron average velocity, average energy, and average energy flux. Input data is required via collision rates for ionization, $\tilde{\nu}_I^{\mathrm{ss}}$, attachment, $\tilde{\nu}_a^{\mathrm{ss}}$, momentum transfer, $\tilde{\nu}_m^{\mathrm{ss}}$, energy transfer, $\tilde{S}_\epsilon^{\mathrm{ss}}$, energy flux transfer, $\tilde{\nu}_\xi^{\mathrm{ss}}$, and higher order tensor product closure approximations, $\theta_m^{\mathrm{SS}} = \langle \mathbf{vv} \rangle_{f_{\mathrm{ss}}}$ and $\theta_\xi^{\mathrm{SS}} = \left\langle \frac{1}{2}mv^2\mathbf{vv} \right\rangle_{f_{\mathrm{ss}}}$. The superscripts SS denote that all input data is computed via velocity averaging over the steady state EVDF found via MC [26, 28] or multi-term kinetic solution of the Boltzmann equation [23, 24, 29, 30], for a given density, and interpolated as a function of the local electron mean energy, $\bar{\epsilon}$. For further details on the moment model used in this study the reader is referred to the recent work of Garland *et al* [13], in addition to other recent studies and reviews on the topic [14–16].

With a moment model for electron transport across a gas–liquid interface detailed above, it can be seen that collisional input rates to the model equations (10)–(13), such as $\tilde{\nu}_m^{\mathrm{ss}}(\bar{\epsilon}, n_0)$ and $S_\epsilon^{\mathrm{ss}}(\bar{\epsilon}, n_0)$, are now functions of mean electron energy, $\bar{\epsilon}$, and the neutral atom density, n_0, which varies in space across the gas–liquid interface. In order to model electron transport across the interface, all steady state averaged collision rates must be known as a function of energy and each value of n_0 across the interface. This data requirement is problematic because to measure this experimentally would be a consuming task, and to compute steady state distribution functions for all densities with coherent scattering and potential screening modifications would be computationally demanding [24–26, 28]. For a solution to this problem, we now seek an approximation to intermediate steady state electron transport properties and collision frequencies using computed dilute gas and liquid extreme transport properties only.

2.2. Interfacial density properties

In order to approximate the transport properties between vapor and liquid extremes, the composition of the interface must be known. For this study, we assume the existence of an equilibrium interfacial density profile formed between dilute gas and liquid phases of some atomic fluid. For this study, non-polar systems (argon, xenon) have been chosen to begin formulating and benchmarking electron transport models between gas and liquid phases. This is in part due to the existence of good experimental data as well as the recent advances in liquid scattering and transport theory [8, 24, 25] which have allowed accurate computation of electron properties in non-polar atomic liquids.

Studies on the existence of an interface between a vapor and liquid surface in equilibrium were modeled in the late 1970s using molecular dynamics (MD) simulations once sufficient computing power became available [31]. Since then, many MD and MC studies have been performed with noble liquids, often modeled using Lennard-Jones (LJ) potentials [6–9]. Key measurables from these studies included equilibrium liquid and vapor densities, surface tension, and interface layer thickness. Kalos *et al* [31] performed MD simulations of argon gas–liquid interface formation, resulting in a well defined interface thickness of approximately $5\sigma_{\mathrm{LJ}}$, where σ_{LJ} is the atomic diameter used in the LJ potential. Later MD and MC studies of various noble liquids [6–8],

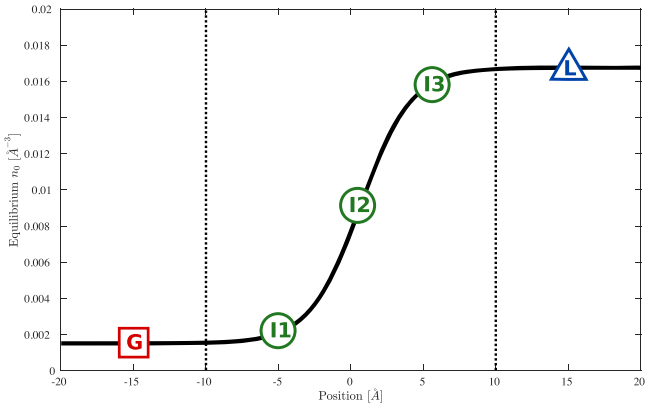

Figure 1. Argon vapor–liquid equilibrium interface as determined by molecular dynamics simulations [6–8]. Labels G and L denote dilute gas and liquid extremities respectively. Labels I1, I2, I3 denote densities at one-quarter, half-way, and three-quarters along the density transition which will be used for benchmarking in section 3.

such as krypton and xenon, confirmed the earlier simulation results of Kalos *et al* [31].

The density profile between liquid and vapor was approximated as a hyperbolic tangent [6–9] as shown in figure 1, where key points on the interface are denoted I1 to I3. In the benchmarking and results to follow, the electron transport properties at these density points between gas and liquid will be approximated.

The ratio between vapor and liquid densities in equilibrium (n_g/n_l) was found to be variable depending on the atomic potentials chosen in the MD simulations [6, 8]. Trokhymchuk and Alejandre [8] studied different cut-off distances for LJ potentials to demonstrate liquid–vapor density ratios of $1/200$ to $1/500$, depending on the cut-off distance from $2.5\sigma_{\mathrm{LJ}}$ to $5.5\sigma_{\mathrm{LJ}}$. In the future, to ensure a sensible liquid–vapor density ratio is employed in transport simulations across the liquid–vapor interface, the highlighted variation in neutral density ratios due to choice of the interaction potential will need to be considered. This cut-off distance is often employed in practice to make computational implementation of the exact LJ potential simpler by assuming a model potential that is fixed to be zero beyond the specified cut-off distance [8].

2.3. Simple model for benchmarking collisions in liquids

Before investigating electron transport in real atomic gases and liquids, it is beneficial to benchmark the performance of a proposed model against simple, well known collision models. For this study we have employed the Percus–Yevick liquid model with structure factor correction of Verlet and Weis [26, 27, 32] to modify a simple gas phase collision model to induce structure and provide a well defined simple liquid model, used often in previous studies [23–25]. The collision (or interaction) model is defined as a hard-sphere elastic momentum transfer cross section $\sigma_m = 6\,\text{Å}^2$ with inelastic step function cross section $\sigma_{\mathrm{inel}}(\epsilon) = 0.1\,\text{Å}^2$, and a threshold energy $\Delta\epsilon_{\mathrm{inel}} = 2\,\mathrm{eV}$. Electron mass and neutral atom mass are defined as $m_e = 5.486 \times 10^{-4}\,\mathrm{amu}$ and $m_0 = 4\,\mathrm{amu}$ respectively, with a neutral background temperature of $T_0 = 300\,\mathrm{K}$.

A range of packing fractions $\phi = 0,\ 0.1,\ 0.2,\ 0.3,\ 0.4$ were used to simulate increasingly dense fluids between a dilute gas, $\phi = 0$, and a final liquid phase, $\phi = 0.4$. For a given known neutral atom density the packing fraction is defined as

$$\phi = \frac{4}{3} r^3 n_0, \tag{17}$$

where r is the hard sphere radius, which can be expressed as $r = \sqrt{\frac{\sigma_m}{\pi}}$ for the hard sphere collision model or approximated by the van der Waal radius for a real atom.

The analytic static structure factor of Verlet and Weis [27] was used in this study, and is defined as

$$S_{\mathrm{VW}}(\Delta k, n_0) = \left(1 + \frac{24\eta(S_1 + S_2 + S_3)}{\Delta k^2}\right)^{-1}, \tag{18}$$

where the terms

$$\begin{aligned} S_1 &= \frac{2}{\Delta k^2}\left(12\frac{\gamma}{\Delta k^2} - \beta\right), \\ S_2 &= \frac{\sin(\Delta k)}{\Delta k}\left(\alpha + 2\beta + 4\gamma - 24\frac{\gamma}{\Delta k^2}\right), \\ S_3 &= \frac{2\cos(\Delta k)}{\Delta k^2}\left(\beta + 6\gamma - 12\frac{\gamma}{\Delta k^2}\right) \\ &\quad - \cos(\Delta k)(\alpha + \beta + \gamma), \end{aligned}$$

are nonlinear functions of the neutral number density via the packing fraction (17), and $\eta = \phi - \frac{\phi^2}{16}$, $\alpha = \frac{(1+2\eta)^2}{(1-\eta)^4}$, $\beta = -6\eta\left(\frac{(1+0.5\eta)^2}{(1-\eta)^4}\right)$, and $\gamma = \frac{\eta\alpha}{2}$.

With well defined properties of an equilibrium vapor–liquid interface and a simple liquid collision interaction model, we now seek to obtain expressions to approximate drift velocities, and thus momentum transfer collision frequencies, for intermediate densities between gas and liquid extremes as depicted in the interface configuration in figure 1.

3. Approximating electron transport at associated intermediate densities

The following section presents the derivation and associated benchmarking of approximations to input electron collision frequencies at intermediate densities between gas and liquid extremes. In order to derive our approximations we take inspiration from dilute gas swarm physics methods for approximating drift velocities in gas mixtures as weighted combinations of each pure constituent gas's drift velocity. These mixture rules initially took the form of Blanc's law [33], which assumed that the EEDF in the gas mixture at a reduced field (E/N) is the same as the EEDF in the pure constituent gases at the same E/N. This type of approximation was later described as a common E/N (CEON) procedure [34]. The CEON concept was extended and improved [34, 35] to the common mean energy (CME) method which assumes that the EEDF in the gas mixture at a

given electron mean energy is the same as the EEDF in the pure constituent gases at the same mean energy.

In what follows, we adapt the CME derivation presented by Jovanovic *et al* [34] and consider steady state momentum and energy balance equations for gas, liquid, and intermediate densities to yield expressions for electron drift velocities at intermediate densities. Drift velocity was chosen as the benchmark variable in this study, as opposed to the collision frequencies needed as moment model input. This was decided because experimentally measuring drift velocity is straightforward compared to collision rates, allowing approximations produced in this study to be verified directly. Further discussion on these dilute gas mixture rules are presented in the appendix.

3.1. Momentum balance method

We first consider the steady state spatially averaged momentum balance form of equation (11) for electrons in a dense fluid, of neutral density n_{int}, within the interfacial region between the gas and liquid extremes, with neutral densities n_g and n_l respectively. We assume the momentum transfer collision frequency is a slowly varying function of electron mean energy and apply first order momentum transfer theory (MTT) [17, 20, 36] to write electron transport as a function of the electron mean energy, and assume there is a one to one relationship between the reduced field and electron mean energy [34]. This yields

$$\frac{e}{m_e}\check{E}_{\text{int}}(\langle\epsilon\rangle_{\text{int}}) = W_{\text{int}}(\langle\epsilon\rangle_{\text{int}})\langle\check{\nu}_m^{\text{int}}\rangle(\langle\epsilon\rangle_{\text{int}}), \tag{19}$$

where $\check{E}_{\text{int}} = E_{\text{int}}/n_{\text{int}}$ is the reduced electric field, W_{int} is the electron drift velocity, and $\langle\check{\nu}_m^{\text{int}}\rangle = \langle\nu_m^{\text{int}}\rangle/n_{\text{int}}$ is the unknown electron reduced momentum transfer frequency in the fluid at this intermediate density. For emphasis, we explicitly write that the steady state transport properties are functions of the mean electron energy, $\langle\epsilon\rangle_{\text{int}}$.

As per the CME method of dilute gas mixture rules [34], we now assume the intermediate momentum transfer rate, $\langle\check{\nu}_m^{\text{int}}\rangle$, can be approximated by a weighted combination of collisions due to gas phase transport and collisions in the liquid extreme evaluated at a common electron mean energy

$$\langle\check{\nu}_m^{\text{int}}\rangle(\langle\epsilon\rangle_{\text{int}}) = x_g\langle\check{\nu}_m^{g}\rangle(\langle\epsilon\rangle_{\text{int}}) + x_l\langle\check{\nu}_m^{l}\rangle(\langle\epsilon\rangle_{\text{int}}), \tag{20}$$

where $\langle\check{\nu}_m^{g,l}\rangle = \langle\nu_m^{g,l}\rangle/n_{\text{int}}$ denotes reduced collision frequencies of electrons in gas and liquid extremes, and the density fractions, $x_{g,l}$, follow the relation

$$x_l = 1 - x_g. \tag{21}$$

These density fractions are determined by defining the intermediate density as a sum of fractions of either density extreme

$$n_{\text{int}} = x_g n_g + x_l n_l, \tag{22}$$

such that we can find an expression for the density fraction

$$x_g = \frac{n_l - n_{\text{int}}}{n_l - n_g}. \tag{23}$$

We now consider the steady state momentum balance equation (19) of electrons in the two gas and liquid extremes taken at the same neutral density, n_{int}, as the interfacial density we seek to approximate

$$\frac{e}{m_e}\check{E}_{g,l}(\langle\epsilon\rangle_{g,l}) = W_{g,l}(\langle\epsilon\rangle_{g,l})\langle\check{\nu}_m^{g,l}\rangle(\langle\epsilon\rangle_{g,l}), \tag{24}$$

where $\langle\epsilon\rangle_{g,l}$ is the electron mean energy, $\check{E}_{g,l}$ is the reduced electric field, and $W_{g,l}$ is the electron drift velocity in either gas or liquid extremes.

We now invoke the CME assumption [34] so that electron transport is described as a function of a common electron mean energy, $\bar{\varepsilon}$, in any intermediate fluid on the interfacial region, or in pure gas or liquid extremes. We may now substitute $\langle\check{\nu}_m^{g,l}\rangle$ from equation (24) and combine equations (20) and (19) to find an expression, similar to the dilute gas mixture rule of Blanc's law [33], but which accounts for electric field variation as a function of mean energy

$$\frac{1}{W_{\text{int}}(\bar{\varepsilon})} = x_g\frac{\check{E}_g(\bar{\varepsilon})}{\check{E}_{\text{int}}(\bar{\varepsilon})}\frac{1}{W_g(\bar{\varepsilon})} + x_l\frac{\check{E}_l(\bar{\varepsilon})}{\check{E}_{\text{int}}(\bar{\varepsilon})}\frac{1}{W_l(\bar{\varepsilon})}, \tag{25}$$

where all steady state drift velocities and reduced fields are interpolated as functions of the local electron mean energy $\bar{\varepsilon}$.

To determine the accuracy of the proposed approximation from momentum balance (25) we now perform benchmark calculations using the simple liquid collision model defined in section 2.3. Using the momentum balance rule (25), steady state drift velocities were approximated for multiple packing fractions $\phi = 0.1, 0.2, 0.3$ using only the properties of the extreme $\phi = 0$ and $\phi = 0.4$ fluids, as per the interface layout in figure 1.

Approximations computed from (25) were compared against accurate results obtained from multi-term solutions of the Boltzmann equation [23–25]. All variables for the gas and liquid extremes were interpolated as functions of electron mean energy, $\bar{\varepsilon}$, using the steady state mean energy of the intermediate density computed from a multi-term kinetic solution [24]. It should be noted that the use of equation (25) necessitates a knowledge of the functional relationship between steady state reduced field and mean energy, $\check{E}_{\text{mix}}(\bar{\varepsilon})$, which in practice would not be known when approximating interfacial transport properties for input to a moment model. For these benchmarking calculations the steady state relationship $\check{E}_{\text{mix}}(\bar{\varepsilon})$ computed from kinetic solutions was used at each intermediate ϕ step; in this way the assumption of decomposing the intermediate collision frequency as a function of gas and liquid extremes can be solely tested.

Results of the benchmark calculations for the momentum balance rule (25) are shown in figure 2 where approximate values of drift velocity are given by the dashed line series and, for comparison, solid lines denote accurate values obtained via multi-term solution of the Boltzmann equation. The accurate benchmark solutions of the Boltzmann equation used in this study are computed via the multi-term solution framework developed by the JCU group. For the formulation and implementation details of this framework the reader is referred to [23–25, 29, 37].

Across all packing fractions it can be seen that the momentum balance rule severely overestimates the

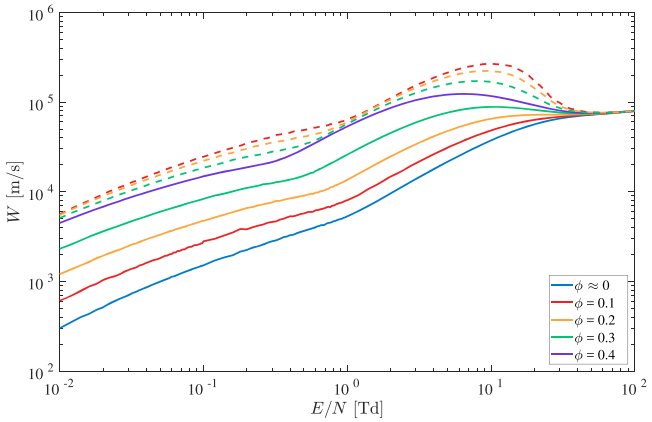

Figure 2. Comparison of electron drift velocities in model simple liquids for $\phi = 0.1$, 0.2, 0.3. Solid lines: multi-term solution of the Boltzmann equation [24]. Dashed lines: computed via approximation (25) derived from momentum balance.

intermediate drift velocity, consistently predicting values above even the $\phi = 0.4$ liquid extremity drift velocities. This is attributed to the failure of the additivity assumption for constructing $\langle \nu_m^{\text{int}} \rangle$, invoked in equation (20). This occurs because the background neutral number density n_0 can no longer be factored out of the intermediate fluid's momentum transfer collision frequency, $\tilde{\nu}_m$, when coherent scattering effects are included.

The introduction of nonlinearity in n_0 can be seen by considering momentum transfer collision frequencies (8) and (9), where the structure modified momentum cross section is derived via an energy integral over the nonlinear static structure factor, in this case the Verlet–Weis analytic form, $S_{\text{VW}}(\Delta k, n_0)$ as per (18). In the dilute gas case, ν_m was directly proportional to n_0 and so some proportionality to n_0 can be reasonably expected when neutral densities are low. However, once coherent scattering effects are important, the nonlinearity of the static structure factor clearly breaks down any simple proportionality relation between $\tilde{\nu}_m$ and n_0. With the momentum balance approximation failing to sufficiently describe intermediate density drift velocities, the assumption invoked in equation (20) requires further improvement.

3.2. Energy balance method

We now consider the steady state spatially averaged form of the energy balance equation (12) for an intermediate density between gas and liquid extremes. As per section 3.1 we apply first order MTT [17, 20, 36] and also assume there is a one to one relationship between the reduced field and electron mean energy [34] to write transport coefficients and collision rates as a function of the electron mean energy, $\langle \epsilon \rangle_{\text{int}}$, i.e.,

$$e\check{E}_{\text{int}}(\langle \epsilon \rangle_{\text{int}})\, W_{\text{int}}(\langle \epsilon \rangle_{\text{int}}) = \left(\langle \epsilon \rangle_{\text{int}} - \frac{3}{2} k_B T_{\text{int}} \right) \times \langle \check{\nu}_e^{\text{int}} \rangle (\langle \epsilon \rangle_{\text{int}}) + \Delta\epsilon_{\text{inel}} \langle \check{\nu}_{\text{inel}}^{\text{int}} \rangle (\langle \epsilon \rangle_{\text{int}}), \tag{26}$$

where we have explicitly separated the elastic and inelastic collision rates, $\langle \check{\nu}_e^{\text{int}} \rangle = \langle \nu_e^{\text{int}} \rangle / n_{\text{int}}$ is the reduced elastic electron energy transfer collision frequency, T_{int} is the temperature of the fluid at an interfacial point, $\Delta\epsilon_{\text{inel}}$ is the inelastic collision threshold energy, and $\langle \check{\nu}_{\text{inel}}^{\text{int}} \rangle = \langle \nu_{\text{inel}}^{\text{int}} \rangle / n_{\text{int}}$ is the reduced electron inelastic energy transfer collision frequency due to internal energy state changes from inelastic threshold collisions[4].

In contrast to section 3.1, we now assume additivity of *energy* transfer collision frequencies for both gas and liquid extremes, evaluated at the interfacial mean energy, $\langle \epsilon \rangle_{\text{int}}$, to approximate the collision frequencies at the intermediate density

$$e\check{E}_{\text{int}}(\langle \epsilon \rangle_{\text{int}})\, W_{\text{int}}(\langle \epsilon \rangle_{\text{int}}) = \left(\langle \epsilon \rangle_{\text{int}} - \frac{3}{2} k_B T_{\text{int}} \right) \times [x_g \langle \check{\nu}_e^{g} \rangle (\langle \epsilon \rangle_{\text{int}}) + x_l \langle \check{\nu}_e^{l} \rangle (\langle \epsilon \rangle_{\text{int}})] + \Delta\epsilon_{\text{inel}} [x_g \langle \check{\nu}_{\text{inel}}^{g} \rangle (\langle \epsilon \rangle_{\text{int}}) + x_l \langle \check{\nu}_{\text{inel}}^{l} \rangle (\langle \epsilon \rangle_{\text{int}})], \tag{27}$$

where $\langle \check{\nu}_e^{g,l} \rangle = \langle \nu_e^{g,l} \rangle / n_{\text{int}}$ denotes reduced electron energy transfer collision frequency with superscripts g, l denoting either the gas or liquid extremes, $\langle \check{\nu}_{\text{inel}}^{g,l} \rangle$ is the reduced inelastic energy transfer collision frequency due to inelastic threshold collisions, and density fractions $x_{g,l}$ are defined as per equations (21)–(23).

To obtain expressions for $\langle \check{\nu}_e^{g,l} \rangle$ in either extreme, we now consider the steady state energy balance equations (26) of electrons in the gas and liquid extremes taken at the same neutral density, n_{int}, as the interfacial density we seek to approximate

$$e\check{E}_{g,l}(\langle \epsilon \rangle_{g,l})\, W_{g,l}(\langle \epsilon \rangle_{g,l}) = \left(\langle \epsilon \rangle_{g,l} - \frac{3}{2} k_B T_{g,l} \right) \times \langle \check{\nu}_e^{g,l} \rangle (\langle \epsilon \rangle_{g,l}) + \Delta\epsilon_{\text{inel}} \langle \check{\nu}_{\text{inel}}^{g,l} \rangle (\langle \epsilon \rangle_{g,l}). \tag{28}$$

If we assume the temperature is constant across all densities in the gas–liquid interface system, and we again invoke the CME assumption to abstract steady state electron transport at all neutral densities as a function of some CME, $\bar{\varepsilon}$, we rearrange (28) to obtain expressions for $\langle \check{\nu}_e^{g,l} \rangle$ and substitute them into (27). It can be shown that the reduced inelastic scattering rates $\langle \check{\nu}_{\text{inel}}^{g,l} \rangle$ cancel out yielding an expression for the drift velocity at the intermediate density

$$W_{\text{int}}(\bar{\varepsilon}) = x_g \frac{\check{E}_g(\bar{\varepsilon})}{\check{E}_{\text{int}}(\bar{\varepsilon})} W_g(\bar{\varepsilon}) + x_l \frac{\check{E}_l(\bar{\varepsilon})}{\check{E}_{\text{int}}(\bar{\varepsilon})} W_l(\bar{\varepsilon}). \tag{29}$$

To establish the accuracy of the energy balance approximation (29), we again performed the same benchmark calculations for the simple Percus–Yevick atomic liquid. Results of this approximation are shown in figure 3, where solid lines denote accurate values obtained via multi-term solution of the Boltzmann equation and approximate values of drift velocity are given by the dashed line series.

In general, the approximation derived from energy balance (29) appears to be a better representation of the intermediate density than the momentum balance method (25). For higher packing fractions $\phi = 0.2$, 0.3 the approximation of drift velocity by (29) demonstrates an excellent agreement

[4] For clarity in our derivation, we have included just one inelastic excitation scattering process. It is straightforward to demonstrate that the following results are unaffected by adding further inelastic scattering processes.

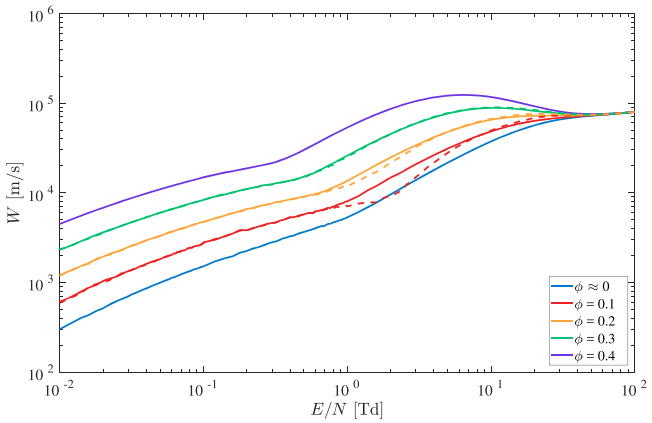

Figure 3. Comparison of electron drift velocities in model simple liquids for $\phi = 0.1, 0.2, 0.3$. Solid lines—multi-term solution of the Boltzmann equation [24]. Dashed lines—computed via approximation (29) derived from energy balance.

with an accurate kinetic solution across all energy ranges. The agreement for the $\phi = 0.1$ case is strong at low and high fields but loses accuracy at intermediate fields of approximately 1–5 Td, where a maximum error of approximately 30% is produced. In this field range the assumption that the energy transfer collision frequency can be approximated by a linear combination of the collision frequencies in gas and liquid extremes, as invoked in (27), appears to be insufficient. The effects of this inaccuracy are very apparent in the $\phi = 0.1$ case in figure 3, and present to a lesser degree in the $\phi = 0.2$ case. This is a reflection of the approximations associated with the first-order MTT used in developing the relation (29) [17, 38]. This inaccuracy could be improved through higher-order MTT if desired.

To explain why an approximation derived from energy balance should perform better than one derived from momentum balance, we recall the modifications of electron transport in gases required to simulate transport in liquid media, outlined in section 2.1. Firstly, inelastic collisions result in largely localized energy transfer between electrons and the background medium, and we assume that these are incoherent scattering events which can be treated by classical dilute gas kinetic theory [23–25]. On the other hand, in the structure modified kinetic theory [23] used to describe electron transport in condensed materials, coherent elastic scattering collisions are important. Since it is elastic scattering that carries the explicit density dependent coherent scattering effects, it is not surprising that momentum transfer is impacted more than energy transfer as the neutral density of the background fluids are increased.

In summary, from a rule based on largely structure independent energy transfer (29) we observe a reasonable approximation to W_{int}, as opposed to an approximation that ignores the nonlinear density effects on momentum transfer (25). With this result, it appears we are better placed to approximate a lumped energy transfer collision frequency of an intermediate fluid by simply assuming additivity of the gas and liquid reduced collision frequencies as per (27). We now seek to correct the approximation derived from momentum balance in the previous section, in order to provide a better approximation to momentum transfer collision rates.

3.3. Modified momentum balance method

We now propose a modified momentum balance approximation rule that aims to explicitly include some of the nonlinear effects of density dependent coherent scattering in the approximation of $\langle \nu_m^{\text{int}} \rangle$. By only considering structure induced coherent scattering effects in this treatment, we henceforth neglect density dependent potential screening effects in the differential cross section (7). Future studies will endeavor to relax this assumption in order to more accurately describe density dependent scattering via interaction potential screening and not just coherent scattering.

To isolate density dependence of the soft condensed phase scattering interaction, we apply first order MTT [17, 20, 36] to evaluate the structure modified momentum transfer cross section as a function of electron mean energy, $\bar{\varepsilon}$,

$$\Sigma_m(\bar{\varepsilon}, n_0) \approx \sigma_m(\bar{\varepsilon}) s(\bar{\varepsilon}, n_0), \tag{30}$$

where $s(\bar{\varepsilon}, n_0)$ is an angle integrated structure factor with explicit n_0 dependence

$$s(\bar{\varepsilon}, n_0) = \frac{1}{2}\int_0^{\pi} S\left(\frac{2}{\hbar}\sqrt{2m_e\bar{\varepsilon}}\,\sin\frac{\chi}{2}, n_0\right)[1 - \cos\chi]\mathrm{d}\chi. \tag{31}$$

In the limit of isotropic scattering the approximations of equations (30) and (31) are exact [17, 36, 38]. Decomposing the structure modified momentum transfer cross section to isolate a density dependence, as per the approximation of equation (30), now allows dense phase collision rates to be approximated via scaling of dilute gas collision rates.

We continue the use of MTT and evaluate the structure modified momentum transfer collision frequency (9) as the dilute gas phase momentum transfer collision frequency multiplied by the angle integrated structure factor each evaluated at the electron mean energy, $\bar{\varepsilon}$,

$$\begin{aligned}\langle \tilde{\nu}_m \rangle(\bar{\varepsilon}, n_0) &\approx n_0\sqrt{\frac{2\bar{\varepsilon}}{m_e}}\,\Sigma_m(\bar{\varepsilon}, n_0),\\ &\approx s(\bar{\varepsilon}, n_0)\langle \nu_m \rangle(\bar{\varepsilon}).\end{aligned}$$

Using this result, we now return to the steady state limit of the momentum balance equation (19), but now make the assertion that instead of simply combining certain fractions of gas and liquid reduced momentum transfer collision frequencies we first normalize each input reduced collision frequency $s_{g,l}$ and then rescale by the intermediate density's s_{int}

$$\begin{aligned}\frac{e}{m_e}\check{E}_{\text{int}}(\bar{\varepsilon}) = W_{\text{int}}(\bar{\varepsilon})\Bigg[&x_g\frac{s_{\text{int}}(\bar{\varepsilon})}{s_g(\bar{\varepsilon})}\langle \check{\nu}_m^g \rangle(\bar{\varepsilon})\\ &+ x_l\frac{s_{\text{int}}(\bar{\varepsilon})}{s_l(\bar{\varepsilon})}\langle \check{\nu}_m^l \rangle(\bar{\varepsilon})\Bigg],\end{aligned} \tag{32}$$

where $s_{g,l,\text{int}}$ are the angle-integrated structure factors for gas and liquid extremes, and the intermediate density

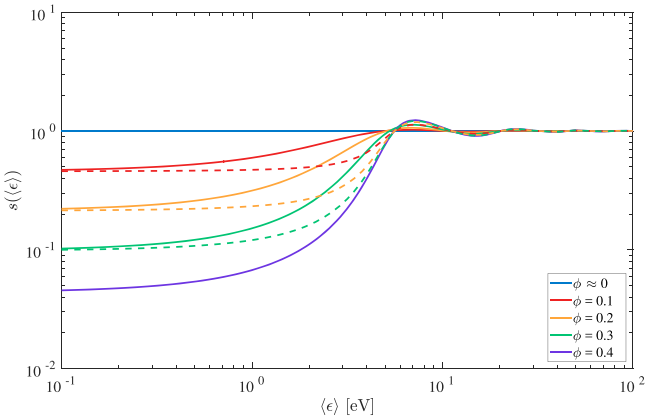

Figure 4. Comparison of approximated angle-integrated structure factors for Percus–Yevick model liquids. Solid lines—exact values via (31). Dashed lines—approximated s via equations (33) and (34).

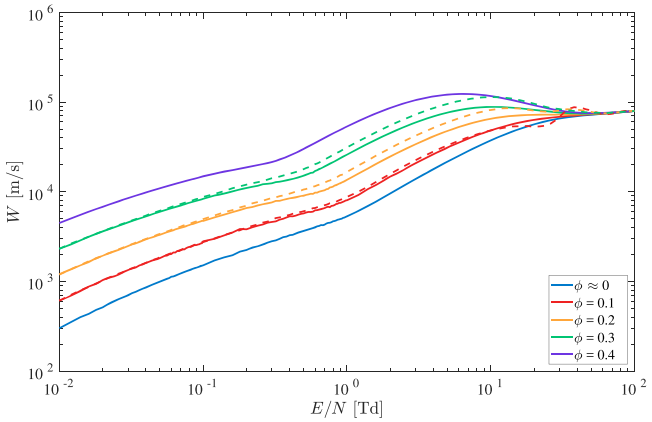

Figure 5. Comparison of electron drift velocities in model simple liquids for $\phi = 0.1, 0.2, 0.3$. Solid lines—multi-term solution of the Boltzmann equation [24]. Dashed lines—computed via approximation (35) derived from structure modified momentum balance.

respectively, all evaluated at a CME $\bar{\varepsilon}$, and density fractions $x_{g,l}$ are defined as per equations (21)–(23).

In practice, when approximating transport properties between gas and liquid extremes over a range of n_0 values, s_{int} must be specified at each point along the interface. Obtaining a function for s_{int} at each point would be very computationally demanding, and is generally not available experimentally. As a result we propose a further approximation for s_{int} as a combination of the limiting gas and liquid angle-integrated structure factors

$$s_{\text{int}} \approx w s_g + (1 - w) s_l, \tag{33}$$

where to ensure the approximation is physically grounded in both the high and low energy limits, the weighting factor, w, is fixed in the low energy limit by

$$w = \frac{S_{\text{int}}(0, n_{\text{int}}) - S_l(0, n_l)}{S_g(0, n_g) - S_l(0, n_l)}, \tag{34}$$

where $S(0)$ is the $\Delta k = 0$ limit of the static structure factor, which is also proportional to the fluid's compressibility.

To benchmark the assumptions used to define equation (33) the approximate and exact angle-integrated structure factors, computed by integrating the analytic Verlet–Weis structure factor, are compared in figure 4, where solid lines denote exact values via integrating (31) and approximate values of s_{int} are given by the dashed line series. We note that for a dilute gas $s_g = 1$ and so we cease to use this variable in the remainder of this treatment.

As expected, the low and high energy limits are fixed exactly, while intermediate energies show some differences once the structure factor begins to peak. By substituting an expression for $\langle \breve{\nu}_m^{g,l} \rangle$ from the momentum balance for either gas or liquid extremes (24) into the intermediate fluid momentum balance (32), and assuming the CME assumption, we yield a modified approximation for drift velocity accounting for some nonlinear density effects

$$\frac{1}{W_{\text{int}}(\bar{\varepsilon})} = x_g s_{\text{int}}(\bar{\varepsilon}) \frac{\breve{E}_g(\bar{\varepsilon})}{\breve{E}_{\text{int}}(\bar{\varepsilon})} \frac{1}{W_g(\bar{\varepsilon})} + x_l \frac{s_{\text{int}}(\bar{\varepsilon})}{s_l(\bar{\varepsilon})} \frac{\breve{E}_l(\bar{\varepsilon})}{\breve{E}_{\text{int}}(\bar{\varepsilon})} \frac{1}{W_l(\bar{\varepsilon})}. \tag{35}$$

We again benchmark this approximation and the results are shown in figure 5, where solid lines denote accurate values obtained via multi-term solution of the Boltzmann equation and approximate values of drift velocity are given by the dashed line series.

It can be seen that this modified momentum balance rule produces a better outcome than the results of the unmodified momentum balance method, shown in figure 2, for all benchmark intermediate densities. As observed for the energy balance approximations in figure 3, the $\phi = 0.2, 0.3$ cases in figure 2 perform consistently well under the modified momentum balance approximation. In contrast to the approximation derived from energy balance, the $\phi = 0.1$ case now demonstrates strong agreement between 1 and 10 Td, demonstrating insensitivity to inelastic scattering effects. Inaccuracies due to equation (35) are observed in the $\phi = 0.1$ case between 10 and 50 Td due to the error in approximating s_{int} as a combination of the gas and liquid extrema structure factors, shown in figure 4.

Despite the noted shortcomings at intermediate fields, the structure-modified drift velocity approximation (35) provides a much better general approximation to W_{int} than the original approximation derived from a simpler momentum balance (25), and demonstrates potential to provide an improved approximation to electron transport at densities between gas and liquid extrema.

3.4. Practical implementation for plasma modeling

So far two approximation rules (29) and (35) have been derived and were demonstrated to have potential in approximating electron drift velocities at intermediate densities between gas and liquid extrema. Each equation is a function

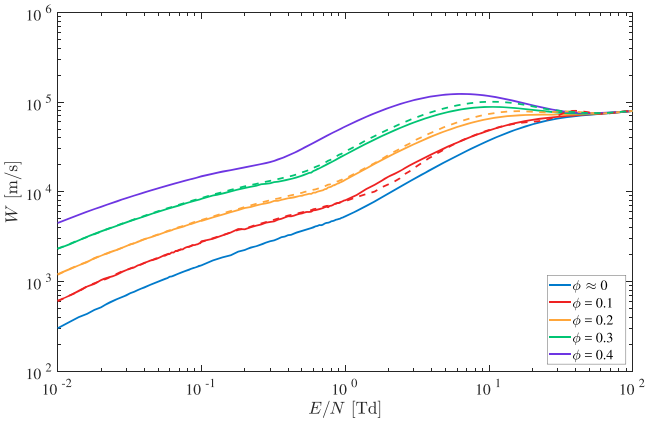

Figure 6. Comparison of electron drift velocities in model simple liquids for $\phi = 0.1, 0.2, 0.3$. Solid lines—multi-term solution of the Boltzmann equation [24]. Dashed lines—computed via the practical approximation (36).

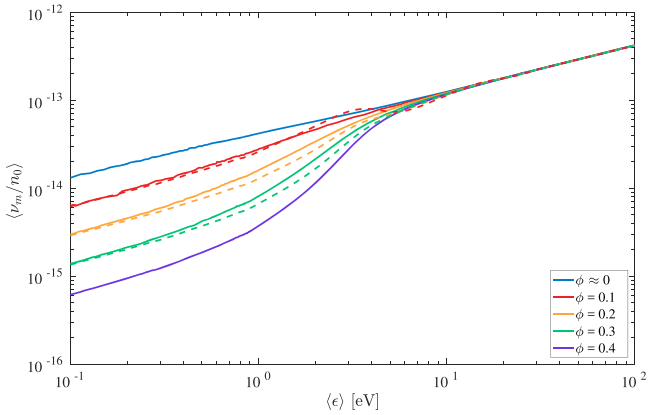

Figure 7. Approximated $\check{\nu}_m^{\text{mix}}$ for multiple packing fractions of PY model liquid. Solid line: exact via multi-term kinetic solution [24], – –: approximation via (37).

of a CME $\bar{\varepsilon}$, and steady state values of $W_{g,l}$ and $\check{E}_{g,l,\text{int}}$ are interpolated at these energies to provide input from either phase extreme. As previously discussed, when used independently, each equation requires knowledge of the steady state relationship between $\check{E}_{\text{int}}$ and $\bar{\varepsilon}$ at the intermediate density between gas and liquid. This requirement is problematic because the gas–liquid interface steady state properties are generally unknown and hence the motivation for this study.

As a way to form an approximation that can be applied in practice, without any knowledge of the steady state transport properties at each intermediate density, we combine the two benchmarked approximation rules from energy balance (29) and modified momentum balance (35) and solve for W_{int}, to eliminate $\check{E}_{\text{int}}$,

$$W_{\text{int}}^2(\bar{\varepsilon}) = \frac{x_g \check{E}_g(\bar{\varepsilon}) W_g(\bar{\varepsilon}) + x_l \check{E}_l(\bar{\varepsilon}) W_l(\bar{\varepsilon})}{x_g s_{\text{int}}(\bar{\varepsilon}) \check{E}_g(\bar{\varepsilon}) \frac{1}{W_g(\bar{\varepsilon})} + x_l \frac{s_{\text{int}}(\bar{\varepsilon})}{s_l(\bar{\varepsilon})} \check{E}_l(\bar{\varepsilon}) \frac{1}{W_l(\bar{\varepsilon})}}. \quad (36)$$

To test the performance of the approximation (36), we now apply it to the benchmark model used throughout this study. The most straightforward measurable that can be used to verify the accuracy of the approximation is the electron steady state drift velocity. Despite not being a direct input in higher order moment models [13–15], it provides a solid measure on the validity of approximations of input collision frequencies. For the Percus–Yevick model of a simple atomic liquid, multiple packing fractions, $\phi = 0.1, 0.2, 0.3$, were used to approximate electron drift velocity and were compared with accurate calculations of the steady state drift velocity as shown in figure 6.

By only specifying the $\Delta k = 0$ analytic limit of the structure factor $S_{\text{VW}}(0, n_{\text{int}})$ of the intermediate densities the combined approximation (36) provides a good representation of the exact results. As discussed earlier, the higher-density fluids perform very well, while the lower-density fluid demonstrates variations from the exact result due to our assumptions on the fluid structure. For packing fractions of $\phi = 0.2, 0.3$ the maximum error observed was 12%, which occurred near the peak value of W before the region of negative differential conductivity (NDC) began. For the lower packing fraction, $\phi = 0.1$, a maximum error of 25% was observed. This approximation was not as accurate because the simple intermediate structure assumptions used in this study did not accurately represent the transition to near-dilute gas phase. An additional encouraging feature of the proposed approximation was the ability to predict structure induced NDC in the model liquids, which has previously been reported to occur at packing fractions above $\phi = 0.2$ [23], using only the analytic $\Delta k = 0$ limit of the static structure factor, and dilute gas and liquid extreme transport data.

3.5. Approximating collision frequencies across an interface

In practice, when simulating electron transport with higher order moment models [13–15] the required inputs are not drift velocities or diffusion coefficients (which could be computed via an Einstein relation once W_{int} is known), but rather reduced collision frequencies. Once an approximate drift velocity is found one may simply compute a reduced momentum transfer frequency via

$$\check{\nu}_m^{\text{int}}(\bar{\varepsilon}) = \frac{e\check{E}_{\text{int}}(\bar{\varepsilon})}{m_e W_{\text{int}}(\bar{\varepsilon})}, \quad (37)$$

in order to approximate the steady state momentum collision rate at the intermediate densities between gas and liquid extremes. The results of using the collision frequency approximation (37) are shown in figure 7 for multiple packing fractions.

It can be seen that the approximation to $\check{\nu}_m^{\text{int}}$ performs quite well without much knowledge of the intermediate fluid's structure and steady state transport properties. Higher density fluids, $\phi = 0.2, 0.3$, demonstrate the best agreement, while the inaccuracies in approximating structure for the $\phi = 0.1$ case are highlighted by the deviation at intermediate energy ranges. This result demonstrates potential for the final approximation rule (36) to be used in conjunction with higher order moment models [13, 14, 16, 39] to provide a foundation for simulating electron transport between gas and liquid extremes as a continuum.

Table 1. Benchmark atomic gas–liquid systems used for validating proposed drift velocity approximation rule against experimental data.

	Liquid— Calc. [24, 25]	Intermediate— Exp. [40]	Gas— Calc. [24, 25]
Argon	85 K	130 K	300 K
Xenon	165 K	230 K	300 K

4. Application to noble gas–liquid systems

In order to further verify the suitability of the derived approximation (36), we now consider application to real gases and liquids. In this section we will seek to use our derived approximation method, with known steady state transport properties of a dilute gas and dense liquid, to estimate steady state electron drift velocities measured in a fluid of intermediate density. In contrast to the previous model where only explicit coherent effects were considered, real atomic systems require additional modifications to the interaction potential associated with varying the neutral density [25]. A classic example of the variation between cross sections at gas and liquid densities is observed in some rare gases and their liquids, where the low-energy Ramsauer minimum found in gas phase cross sections is suppressed and eventually completely non-existent as the liquid density increases [25]. As a result of the complex scattering variations from gas to liquid states, in conjunction with accessible experimental data, liquid argon and liquid xenon were chosen for comparison in this study.

Experimental data of Gushchin *et al* [40] for drift velocity, electric field, and mean energy of electrons in liquid argon and liquid xenon were digitized as a basis for experimental validation of the proposed approximation (36). This data set was chosen over other existing data sets [41–43] because an approximation to the electron mean energy, scaled from measurements of the characteristic energy D/μ, was included in the original study and so provided the necessary mean energy input needed to use our derived approximations. Table 1 outlines the approximate gas to liquid transition assumed for each atomic fluid.

As opposed to the Percus–Yevick model atomic liquid, temperature, T, as well as neutral atom density, n_0, varies between the densities used in experiment. In order to account for this, the neutral densities at each temperature were calculated by interpolating the argon and xenon saturated liquid curves as a function of T [44, 45].

Dilute gas neutral density was approximated as being 300 times smaller than the liquid extreme neutral density based on the equilibrium liquid-gas density ratios found in MD simulations of LJ liquids [6–9].

In contrast to the simplified collision model used in the benchmark system in the previous section, each real fluid in table 1 was measured at different temperatures as well as densities. We note that a modification to the approximation method (36) is required to account for varying temperatures and densities. To account for temperature variation we slightly modify the derivation of the approximation (29) via energy balance (26) to allow thermal components, $\frac{3}{2}k_BT$, to vary between the gas, liquid, and intermediate densities.

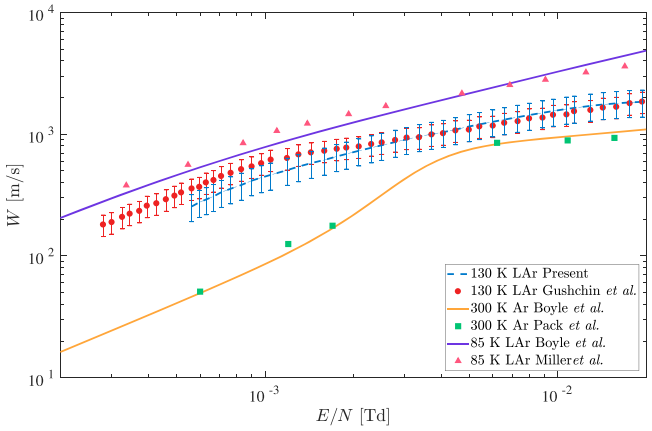

Figure 8. Electron drift velocity in liquid argon at 130 K. Present approximation computed via equation (38) compared with experimental results of Gushchin *et al* [40]. Reference data: Boyle *et al* [24, 46], Miller *et al* [48], Pack *et al* [47].

Assuming the same CME assumption as previous derivations, and allowing $T_g \neq T_{\text{int}} \neq T_l$ we find ratios of the CME minus thermal components do not cancel in the approximation derived from energy balance, and we yield a temperature-modified approximation rule

$$W_{\text{int}}^2(\bar{\varepsilon}) = \frac{\left(x_g \frac{\bar{\varepsilon}-\frac{3}{2}k_BT_{\text{int}}}{\bar{\varepsilon}-\frac{3}{2}k_BT_g}\check{E}_g(\bar{\varepsilon})W_g(\bar{\varepsilon}) + x_l \frac{\bar{\varepsilon}-\frac{3}{2}k_BT_{\text{int}}}{\bar{\varepsilon}-\frac{3}{2}k_BT_l}\check{E}_l(\bar{\varepsilon})W_l(\bar{\varepsilon})\right)}{x_g s_l(\bar{\varepsilon})\check{E}_g(\bar{\varepsilon})W_l(\bar{\varepsilon}) + x_l\check{E}_l(\bar{\varepsilon})W_g(\bar{\varepsilon})} \times \frac{s_l(\bar{\varepsilon})W_g(\bar{\varepsilon})W_l(\bar{\varepsilon})}{s_{\text{int}}(\bar{\varepsilon})}. \tag{38}$$

To ensure accurate input data to our approximation method (38), multi-term solutions of Boltzmann's equation [24, 25] were computed to obtain transport properties for argon and xenon in both dilute gas and liquid extreme conditions. In low density dilute gas and high density liquid states, electron scattering cross sections were taken from the recent *ab initio* refinements that take into account density dependent scattering and screening effects [25, 46] to obtain increased accuracy. To demonstrate the validity of the calculated transport data in gas and liquid extremes, comparison against experimental results is included in figures 8 and 9. Gas phase drift velocity measurements are taken from the work of Pack *et al* [47], while liquid argon and liquid xenon measurements are taken from Miller *et al* [48] and Huang and Freeman [42] respectively.

The angle-integrated structure factors for the liquid extrema and the intermediate fluid, s_l and s_{mix}, were approximated as per the benchmark model atomic liquid used in section 3.3. For liquid argon and xenon we evaluate the analytic static structure factor expression of Verlet and Weis (18) using relevant parameters for argon and xenon, because it has been shown that despite the complex interaction at high densities the expression of Verlet and Weis is a good approximation to the structure factor for noble liquids [8, 26].

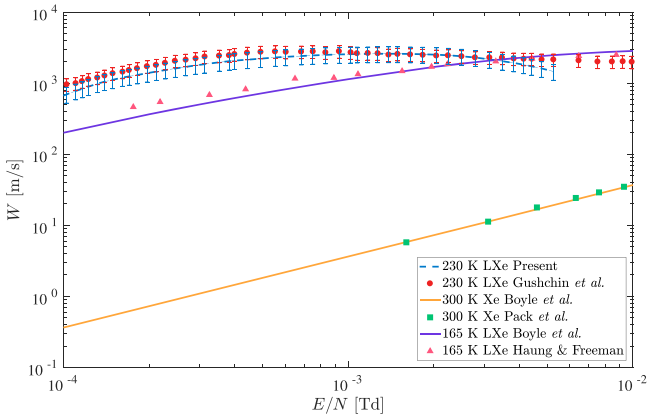

Figure 9. Electron drift velocity in liquid xenon at 230 K. Present approximation computed via equation (38) compared with experimental results of Gushchin *et al* [40]. Reference data: Boyle *et al* [24, 25], Huang and Freeman [42], Pack *et al* [47].

With accurate data for gas and liquid extremes, and a temperature modification to the approximation rule (38), we now compare the approximation of the steady state drift velocity at an intermediate temperature/density for both liquid argon and liquid xenon against experimental results of Gushchin *et al* [40]. The results are shown in figures 8 and 9.

From the experimental work of Gushchin *et al* [40] errors of approximately 5% each were quoted for measurement of the drift velocity and applied electric field, and errors of approximately 10% was quoted for the computation of electron mean energy. Carrying these errors through the approximations used in this study we include estimated error bars on each line series for the intermediate drift velocities in figures 8 and 9.

In figures 8 and 9, we see good agreement between the approximate values computed via (38) and experimental measurements within the uncertainties displayed. Despite no knowledge of the intermediate steady state transport properties, the complexities of the electron scattering cross section changing between gas and liquid densities, and an approximate treatment of the effects of structure, both approximations provide a good estimation of the drift velocity in the intermediate fluid densities.

The liquid argon approximation provides the best fit of the two atomic systems considered, with a strong qualitative and functional agreement between experiment and calculated data. An encouraging feature of the liquid argon result is the ability of the approximation to demonstrate a gradient change that occurs at roughly 10^{-3} Td. For liquid xenon, the prediction of NDC at low fields is also an encouraging result of our approximation. The magnitude and window of reduced fields at which the approximated NDC occurs is not exactly replicated, but the ability of the approximation rule to predict NDC by employing very simple structure assumptions shows the utility of the proposed approximation. Future improvements in approximating the intermediate density structure effects via experimental structure factors, and including interaction potential screening effects, may yield even greater accuracy in approximating complex transport behavior.

5. Conclusions

In summary, we have proposed expressions (36) and (38) to approximate electron transport at intermediate densities in the gas–liquid interfacial region from data in the gas and liquid extreme phases only. To formulate the approximation method we have extended well known mean energy dependent gas phase mixture rules into high density fluids which exhibit nonlinear density dependent transport properties. We have applied a simple analytic structure modification to account for nonlinear density effects on electron momentum transfer, and benchmarked this modification with simple atomic liquid models. Following analysis of structure induced momentum transfer effects, an approximation derived from energy balance between electrons and structured media was benchmarked and demonstrated suitable accuracy for a wide range of reduced fields. Improved accuracies could be achieved with higher-order MTT [17, 38]. Finally, to form a practical approximation rule that can be used without any knowledge of the reduced field's dependence on mean energy, approximations derived from energy balance and modified momentum balance were combined and the subsequent expression was benchmarked.

Steady state transport properties of a simple atomic liquid model plus experimental data of argon and xenon liquids were assembled for comparison. By applying the final combined drift velocity approximation (36), and (38) for including temperature variation in the experimental benchmarks, we have demonstrated the utility of our approximation in predicting drift velocities of intermediate fluids between gas and liquid extremes. We subsequently demonstrated that reduced momentum collision frequencies can be approximated with sufficient accuracy, to serve as input data in higher order electron moment modeling. For the majority of model and experimental gases and liquids the qualitative agreement between approximations and known results was strong. Despite the encouraging performance of the proposed approximation rule, comparison against argon and xenon experimental results demonstrated the complex interaction potentials of real liquids pose a challenge and further study should be carried out on including low-energy screening effects into the approximation of intermediate structure factors, s_{mix}. In addition, further enhancements on the implementation of an angle-integrated structure factor should be studied to account for the structure of even more complex liquids, such as polar molecular liquids like water.

Acknowledgments

NG acknowledges financial support from the Australian Government through the Australian Postgraduate Award, and JCU through the HDR Research Enhancement Scheme.

Appendix. Dilute gas mixture rules

To provide the foundation for an approximation of electron collision rates at intermediate densities between a gas and liquid, methods of approximating drift velocities in dilute gas mixtures were reviewed. Various rules have been used in literature, but all are based on the premise of density fractions, $x_\alpha = n_\alpha/n_{\text{total}}$, computed for each constituent gas being used to scale steady state drift velocities of each constituent gas to provide an approximate of the mixture's steady state transport data.

A.1. Blanc's law

The origin of mixing rules in gas phase charged particle transport can be traced to Blanc's empirical law [33]

$$\frac{1}{W_{\text{mix}}\left(\frac{E}{n_0}\right)} = \sum_\alpha \frac{x_\alpha}{W_\alpha\left(\frac{E}{n_0}\right)}, \tag{39}$$

where W_{mix} is the mixture drift velocity, x_α is the density fraction of gas α such that $\sum_\alpha x_\alpha = 1$, and W_α is the drift velocity in gas α. All drift velocities are evaluated at a common value of reduced electric field, E/n_0; which has since been termed a common E/n_0 (CEON) approach [34].

By the mid 20th century experimental results necessitated modifications to Blanc's law,

$$\frac{1}{W_{\text{mix}}\left(\frac{E}{n_0}\right)} = \sum_\alpha \frac{x_\alpha}{W_\alpha\left(\frac{E}{n_0}\right)} + \delta_B\left(\frac{E}{n_0}\right), \tag{40}$$

where δ_B is some deviation from the original law to include higher order effects and inelastic collisions [34, 49, 50]. Multiple approaches to computing deviations were presented, from rigorous kinetic theory arguments to empirical observations based on new experimental observations. It was shown that Blanc's law was suitable for approximating ion transport in gas mixtures, whereas it failed significantly for electron transport, without severe modifications to the original law [34, 35, 50–52].

The breakdown of Blanc's law for electrons can be understood as a failing of the following two assumptions:

(i) that electron impact cross sections can be added in simple linear combinations at a given value of E/n_0 [49], and
(ii) the steady state EEDF is the same for each gas, and the combination mixture, at a given value of E/n_0 [34].

In general, these assumptions will fail owing to the rapidly varying electron mean energy with increasing E/n_0, and the strong dependence of energy transfer on inelastic collisions, which may occur at vastly different field ranges for different gases. These failings of the CEON method led to an alternative mixing rule based on a CME as proposed by Chiflikian [35].

A.2. CME procedure

The CME rule is in the spirit of modern plasma moment modeling in the sense that transport is defined as a function of charged particle mean energy $\bar{\varepsilon}$ [14, 15, 20, 53–55], instead of the reduced field E/n_0. Two variations of a CME rule may be derived from the steady state momentum and energy balance equations for charged particle transport in a plasma to yield two slightly different equations, corresponding to either momentum ($p = +1$) or energy balance ($p = -1$)

$$1 = \sum_\alpha \frac{\check{E}_\alpha(\bar{\varepsilon})}{\check{E}_{\text{mix}}(\bar{\varepsilon})}\left[\frac{W_{\text{mix}}(\bar{\varepsilon})}{W_\alpha(\bar{\varepsilon})}\right]^p,$$

where $\check{E}_{\text{mix}} = E_{\text{mix}}/n_0$ of the mixture, $\check{E}_\alpha = E_\alpha/n_0$ in gas α, W_{mix} is the drift velocity in the mixture, and W_α is the drift velocity in gas α. All terms are evaluated at the same value of mean energy $\bar{\varepsilon}$.

Adopting either of the two CME approximations was shown to be suitable for both ions and electrons in various gas mixtures. In contrast to Blanc's Law, inelastic collisions are natively included in the general theory [34, 35]. Furthermore, the accuracy of the rule is also not restricted to a two-term EEDF theory, as arbitrary steady state EEDFs are assumed in the derivation [34].

ORCID iDs

N A Garland https://orcid.org/0000-0003-0343-0199
G J Boyle https://orcid.org/0000-0002-8581-4307
D G Cocks https://orcid.org/0000-0002-9943-7100
R D White https://orcid.org/0000-0001-5353-7440

References

Q1

[1] Babaeva N Y, Tian W and Kushner M J 2014 The interaction between plasma filaments in dielectric barrier discharges and liquid covered wounds: electric fields delivered to model platelets and cells *J. Phys. D: Appl. Phys.* **47** 235201
[2] Bruggeman P J *et al* 2016 Plasma–liquid interactions: a review and roadmap *Plasma Sources Sci. Technol.* **25** 053002
[3] Lietz A M and Kushner M J 2016 Air plasma treatment of liquid covered tissue: long timescale chemistry *J. Phys. D: Appl. Phys.* **49** 425204
[4] Richmonds C, Witzke M, Bartling B, Lee S W, Wainright J, Liu C C and Sankaran R M 2011 Electron-transfer reactions at the plasma–liquid interface *J. Am. Chem. Soc.* **133** 17582–5
[5] Gopalakrishnan R, Kawamura E, Lichtenberg A J, Lieberman M A and Graves D B 2016 Solvated electrons at the atmospheric pressure plasma–water anodic interface *J. Phys. D: Appl. Phys.* **49** 295205
[6] Chapela G A, Saville G, Thompson S M and Rowlinson J S 1977 Computer simulation of a gas–liquid surface. Part 1 *J. Chem. Soc. Faraday Trans.* II **73** 1133–44
[7] Lee D J, Telo da Gama M M and Gubbins K E 1984 The vapour–liquid interface for a Lennard-Jones model of argon–krypton mixtures *Mol. Phys.* **53** 1113–30
[8] Trokhymchuk A and Alejandre J 1999 Computer simulations of liquid/vapor interface in Lennard-Jones fluids: some questions and answers *J. Chem. Phys.* **111** 8510

[9] Yi P, Poulikakos D, Walther J and Yadigaroglu G 2002 Molecular dynamics simulation of vaporization of an ultra-thin liquid argon layer on a surface *Int. J. Heat Mass Transfer* **45** 2087–100

[10] Bruggeman P and Leys C 2009 Non-thermal plasmas in and in contact with liquids *J. Phys. D: Appl. Phys.* **42** 053001

[11] Lindsay A, Graves D and Shannon S 2016 Fully coupled simulation of the plasma liquid interface and interfacial coefficient effects *J. Phys. D: Appl. Phys.* **49** 1–23

[12] Mariotti D, Patel J, Švrček V and Maguire P 2012 Plasma–liquid interactions at atmospheric pressure for nanomaterials synthesis and surface engineering *Plasma Process. Polym.* **9** 1074–85

[13] Garland N A, Cocks D G, Boyle G J, Dujko S and White R D 2017 Unified fluid model analysis and benchmark study for electron transport in gas and liquid analogs *Plasma Sources Sci. Technol.* **26**

Q2

[14] Becker M M, Kählert H, Sun A, Bonitz M and Loffhagen D 2016 Advanced fluid modelling and PIC/MCC simulations of low-pressure ccrf discharges *Plasma Sources Sci. Technol.* **26** 044001

[15] Markosyan A H, Teunissen J, Dujko S and Ebert U 2015 Comparing plasma fluid models of different order for 1D streamer ionization fronts *Plasma Sources Sci. Technol.* **24** 065002

[16] Dujko S, Markosyan A H, White R D and Ebert U 2013 High-order fluid model for streamer discharges: I. Derivation of model and transport data *J. Phys. D: Appl. Phys.* **46** 475202

[17] Robson R, White R and Hildebrandt M 2017 *Fundamentals of Charged Particle Transport in Gases and Condensed Matter* (*Monograph Series in Physical Sciences*) (Boca Raton, FL: CRC Press)

[18] Boeuf J P and Pitchford L C 1995 Two-dimensional model of a capacitively coupled rf discharge and comparisons with experiments in the Gaseous Electronics Conference reference reactor *Phys. Rev.* E **51** 1376–90

[19] Hagelaar G J M and Kroesen G M W 2000 Speeding up fluid models for gas discharges by implicit treatment of the electron energy source term *J. Comput. Phys.* **159** 1–12

[20] Robson R E, White R D and Lj Petrović Z 2005 Colloquium: physically based fluid modeling of collisionally dominated low-temperature plasmas *Rev. Mod. Phys.* **77** 1303–20

[21] Robson R E, Nicoletopoulos P, Hildebrandt M and White R D 2012 Fundamental issues in fluid modeling: direct substitution and aliasing methods *J. Chem. Phys.* **137**

[22] Turner M M, Derzsi A, Donkó Z, Eremin D, Kelly S J, Lafleur T and Mussenbrock T 2013 Simulation benchmarks for low-pressure plasmas: capacitive discharges *Phys. Plasmas* **20**

[23] White R D and Robson R E 2011 Multiterm solution of a generalized Boltzmann kinetic equation for electron and positron transport in structured and soft condensed matter *Phys. Rev.* E **84** 1–10

[24] Boyle G J, Cocks D G, Tattersall W J, McEachran R P, White R D, Cocks D G, McEachran R P and White R D 2017 A multi-term solution of the space-time Boltzmann equation for electrons in gases and liquids *Plasma Sources Sci. Technol.* **26** 24007

[25] Boyle G J, McEachran R P, Cocks D G, Brunger M J, Buckman S J, Dujko S and White R D 2016 *Ab initio* electron scattering cross-sections and transport in liquid xenon *J. Phys. D: Appl. Phys.* **49** 355201

[26] Tattersall W J, Cocks D G, Boyle G J, Buckman S J and White R D 2015 Monte Carlo study of coherent scattering effects of low-energy charged particle transport in Percus–Yevick liquids *Phys. Rev.* E **91** 43304

[27] Verlet L and Weis J 1972 Equilibrium theory of simple liquids *Phys. Rev.* A **5** 939

[28] Dujko S, White R D and Lj Petrovic Z 2008 Monte Carlo studies of non-conservative electron transport in the steady-state Townsend experiment *J. Phys. D: Appl. Phys.* **41** 245205

[29] White R D, Robson R E, Dujko S, Nicoletopoulos P and Li B 2009 Recent advances in the application of Boltzmann equation and fluid equation methods to charged particle transport in non-equilibrium plasmas *J. Phys. D: Appl. Phys.* **42** 194001

[30] Becker M M and Loffhagen D 2013 Derivation of moment equations for the theoretical description of electrons in nonthermal plasmas *Adv. Pure Math.* **03** 343–52

[31] Kalos M H, Percus J K and Rao M 1977 Structure of a liquid–vapor interface *J. Stat. Phys.* **17** 111–36

[32] Lekner J 1967 Motion of electrons in liquid argon *Phys. Rev.* **158** 130–7

[33] Blanc A 1908 Recherches sur les mobilités des ions dans les gaz *J. Phys. Théor. Appl.* **7** 825–39

[34] Jovanović J V, Vrhovac S B and Lj Petrović Z 2004 Application of Blanc's law at arbitrary electric field to gas density ratios *Eur. Phys. J.* D **28** 91–9

[35] Chiflikian R V 1995 The analog of Blanc's law for drift velocities of electrons in gas mixtures in weakly ionized plasma *Phys. Plasmas* **2** 3902–9

[36] Robson R E and Ness K F 1986 Velocity distribution function and transport coefficients of electron swarms in gases: spherical-harmonics decomposition of Boltzmanns equation *Phys. Rev.* A **33** 2068–77

[37] White R D, Robson R E, Ness K F and Li B 1999 Charged-particle transport in gases in electric and magnetic fields crossed at arbitrary angles: multiterm solution of Boltzmann's equation *Phys. Rev.* E **27** 1249

[38] Boyle G J, White R D, Robson R E, Dujko S and Lj Petrovic Z 2012 On the approximation of transport properties in structured materials using momentum-transfer theory *New J. Phys.* **14**

[39] Becker M M and Loffhagen D 2013 Enhanced reliability of drift-diffusion approximation for electrons in fluid models for nonthermal plasmas *AIP Adv.* **3** 12108

[40] Gushchin E M M, Kruglov A A A and Obodovskii I M M 1982 Electron dynamics in condensed argon and xenon *Sov. Phys.-JETP* **55** 650

[41] Atrazhev V M, Berezhnov A V, Dunikov D O, Chernysheva I V, Dmitrenko V V and Kapralova G 2005 Electron transport coefficients in liquid xenon *IEEE Int. Conf. on Dielectric Liquids, 2005 (ICDL 2005)* pp 1–4

[42] Huang S and Freeman G R 1978 Electron mobilities in gaseous, critical, and liquid xenon: density, electric field, and temperature effects: quasilocalization *J. Chem. Phys.* **68** 1355–62

[43] Huang S S-S and Freeman G R 1978 Density and temperature effects on electron mobilities in gaseous, critical and liquid n-hexane, cyclohexane, and cyclopentane *Can. J. Chem.* **56** 2388–95

[44] Sifner O and Klomfar J 1994 Thermodynamic properties of xenon from the triple point to 800 K with pressures up to 350 MPa *J. Phys. Chem. Ref. Data* **23** 63–152

[45] Stewart R B and Jacobsen R T 1989 Thermodynamic properties of argon from the triple point to 1200 K with pressures to 1000 MPa *J. Phys. Chem. Ref. Data* **18** 639–798

[46] Boyle G J, McEachran R P, Cocks D G and White R D 2015 Electron scattering and transport in liquid argon *J. Chem. Phys.* **142** 1–13

[47] Pack J L, Voshall R E, Phelps A V and Kline L E 1992 Longitudinal electron diffusion coefficients in gases: noble gases *J. Appl. Phys.* **71** 5363–71

[48] Miller L S, Howe S and Spear W E 1968 Charge transport in solid and liquid Ar, Kr, and Xe *Phys. Rev.* **166** 871–8

[49] Sandler S I and Mason E A 1968 Kinetic theory deviations from Blanc's law of ion mobilities *J. Chem. Phys.* **48** 2873–5
[50] Milloy H B and Robson R E 1973 The mobility of potassium ions in gas mixtures *J. Phys.* B **6** 1139
[51] Biondi M A and Chanin L M 1961 Blanc's law-ion mobilities in helium–neon mixtures *Phys. Rev.* **122** 843–7
[52] Šašić O, Jovanović J, Lj Petrović Z, de Urquijo J, Castrejón-Pita J R, Hernández-Ávila J L and Basurto E 2005 Electron drift velocities in mixtures of helium and xenon and experimental verification of corrections to Blanc's law *Phys. Rev.* E **71** 46408
[53] Nicoletopoulos P, Robson R E and White R D 2012 Fluid-model analysis of electron swarms in a space-varying field: nonlocality and resonance phenomena *Phys. Rev.* E **85** 1–7
[54] Sigeneger F and Loffhagen D 2016 Fluid model of a single striated filament in an RF plasma jet at atmospheric pressure *Plasma Sources Sci. Technol.* **25** 035020
[55] Hagelaar G J M and Pitchford L C 2005 Solving the Boltzmann equation to obtain electron transport coefficients and rate coefficients for fluid models *Plasma Sources Sci. Technol.* **14** 722–33